J. Fluid Mech. (2015), *vol.* 769, *pp.* 522–540.
doi:10.1017/jfm.2015.126

A balloon bursting underwater

A. R. Vasel-Be-Hagh[1],†, R. Carriveau[1] and D. S.-K. Ting[1]

[1]Turbulence and Energy Laboratory, Lumley Centre for Engineering Innovation, University of Windsor, Ontario, Canada N9B 3P4

(Received 6 May 2014; revised 20 February 2015; accepted 24 February 2015; first published online 25 March 2015)

A buoyant vortex ring produced by an underwater bursting balloon was studied experimentally. The effect of dimensionless surface tension on characteristics including rise velocity, rate of expansion, circulation, trajectory, and lifetime of the vortex ring bubble was investigated. Results showed reasonable agreement with the literature on vortex rings produced by conventional approaches. It was observed that as the dimensionless surface tension increased, the rise velocity, the circulation and consequently the stability of the vortex ring bubble increased; however, the rate of expansion tends toward constant values. A semi-analytical model is proposed by modifying the drag-based model presented by Sullivan *et al.* (*J. Fluid Mech.*, vol. 609, 2008, pp. 319–347) to make it applicable to buoyant vortex rings. The modified model suggests that the vortex ring expansion is essentially due to the buoyancy force. An expression is also derived for the circulation in terms of the initial volume of the balloon and the depth at which the balloon bursts.

Key words: bubble dynamics, vortex dynamics

1. Introduction

There is a fundamental difference in the physics of vortex rings depending on whether they are buoyant or not. According to Reynolds (1876), the impulse P of a non-buoyant vortex ring in a viscous fluid is constant. Hence, considering Turner's (1957) impulse equation $P = \rho\Gamma\pi R^2$ and the fact that vortex rings expand as they advance, the circulation Γ of a non-buoyant vortex ring decreases with time. In the case of buoyant vortex rings, also called vortex ring bubbles, impulse increases under the action of the buoyancy force; therefore, the circulation remains constant. Non-buoyant vortex rings have been extensively studied for more than a century; the buoyant vortex rings, however, have received relatively less attention. Nevertheless, a number of seminal theoretical (e.g. Turner 1957; Walters & Davidson 1963; Pedley 1968; Joseph, Funada & Wang 2007), experimental (e.g. Turner 1957; Walters & Davidson 1963) and numerical (e.g. Lundgren & Mansour 1991; Cheng, Lou & Lim 2013) contributions have been made concerning the general properties and the stability of buoyant vortex rings. One of the latest studies on the vortex ring bubbles was the lattice Boltzmann simulation conducted by Cheng *et al.* (2013). The main motivation of their study was to assess whether the ring bubble continues to expand

† Email address for correspondence: vaselb@uwindsor.ca

while the rise velocity decreases, as was predicted by Turner (1957), Walters & Davidson (1963), Pedley (1968) and Lundgren & Mansour (1991), or ultimately a steady state is achieved at which the ring radius and rise velocity become constant, as was predicted by Joseph *et al.* (2007). Cheng *et al.* (2013) found that, in contrast to Joseph *et al.*'s (2007) prediction, the ring radius increases and the rising velocity decreases with time until the vortex ring becomes unstable and breaks down into small spherical cap bubbles.

For further investigation, we extended the model proposed by Sullivan *et al.* (2008) to include buoyant vortex rings and, unexpectedly, achieved a steady-state solution suggesting that similar to spherical bubbles, the vortex ring bubbles eventually attain a constant velocity, as was predicted by Joseph *et al.* (2007). This implication prompted us to experimentally assess whether the modified model matches with reality or not. Another major motivation for the present work was the conspicuous lack of an investigation concerning the flow produced by the bursting of balloons used increasingly in maritime energy storage and salvage applications. According to the literature (e.g. Walker *et al.* 1987; Sullivan *et al.* 2008; Hershberger, Bolster & Donnelly 2010; Gan, Dawson & Nickels 2012) the common technique for the generation of a vortex ring bubble is the rapid ejection of fluid into a water tank through an orifice exit. In other words, the initial source of energy is kinetic, whereas the vortex ring bubbles studied herein are powered by the potential energy initially stored in the underwater balloons. Beyond this, an investigation exploring high-Bond-number vortex rings was not evident in the literature. A secondary motivation for the present work was to close this gap by studying vortex rings up to $Bo = 1000$ produced by large balloons bursting in a 25 m^{-3} water tank.

Before the subject of a balloon bursting underwater can be discussed, it is important first to briefly review some basic characteristics of buoyant vortex rings described in the literature. Then, the dynamics of vortex ring bubbles will be characterized through a semi-analytical model based on the concept of drag. Afterwards, the setup and procedure of the experiment are described. At the end, results are presented and discussed.

2. Buoyant vortex rings

Turner (1957) developed one of the earliest analytical theories about vortex ring bubbles by invoking two fundamental assumptions. First, vorticity generated on the bubble surface was assumed to be confined within a region which never extends to the symmetry axis of the vortex ring; therefore, no vorticity is cancelled due to diffusion across the axis of symmetry (OO' in figure 1). As sketched in figure 1, a region of rotational flow rising along with the vortex ring was postulated; Turner illustrated this moving region via a shadowgraph picture of a buoyant vortex ring, see Turner (1957, figure 7). Second, Turner (1957) assumed that no vorticity was diffused across the boundary of the bulk fluid region $\boldsymbol{B}$, that is, no vorticity was lost to a wake. In view of the aforementioned assumptions, circulation remains constant since vorticity is constant, and the viscous effect is negligible in the force balance since there is no momentum loss in a viscous wake. These assumptions also underlay some later theoretical and numerical analyses such as those of Walters & Davidson (1963), Pedley (1968) and Lundgren & Mansour (1991). Turner (1957) predicted that a ring bubble expands radially as it rises;

$$R_T = \left(R_0^2 + \frac{Ft}{\pi\Gamma}\right)^{1/2} \tag{2.1}$$

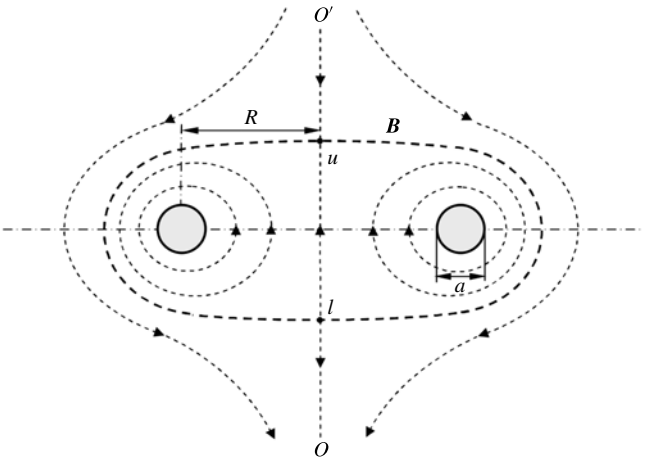

FIGURE 1. $\boldsymbol{B}$ is the boundary of the bulk fluid carried along with the vortex ring; within this region the flow is rotational whereas the ambient flow is irrotational. The shape of the boundary $\boldsymbol{B}$ depends on the ratio R/a, where R and a respectively represent the ring and core radii; at $R/a < 14$, it looks like an oblate spheroid; as R/a increases points u and l approach each other and eventually meet at $R/a = 86$, forming a toroidal region.

where R_0 is the initial radius of the vortex ring, t stands for time and F is defined as $g\Omega(\rho - \rho')/\rho$ in which Ω is volume of the vortex ring, ρ is the density of water and ρ' is the density of air. The rising velocity, however, decreases as

$$u_T = \frac{c\Gamma}{R_T} \tag{2.2}$$

where c is a constant. In the present paper, § 5.2, a comparison is drawn with the expansion of the vortex ring bubble generated by the bursting balloon and those given by (2.1). In addition to this analytical theory, Turner (1957) also performed some experiments and realized the rather unexpected conclusion that for a given circulation, increasing the buoyancy force decreases the rising velocity. Furthermore, he found that increasing the buoyancy force gives a greater rate of expansion; our mathematical model presented in § 3.2 confirms this observation by demonstrating that the ring expansion is basically caused by the buoyancy force.

Turner's (1957) findings on the general properties of a vortex ring were later confirmed by Pedley's (1968) analytical solution. Pedley (1968) demonstrated that the vortex ring radius increases as t and the rising velocity decreases as $t^{-1/2}$ which is in accordance with (2.2). Besides tracing these properties, he investigated the stability of the vortex ring and predicted that it will eventually break up since the stabilizing influence of the circulation decreases as the velocity at the bubble surface decreases through the action of viscosity. Further to this, the destabilizing effect of surface tension increases as the diameter of the core decreases with the vortex ring expansion. He expressed the critical time t_c, the time at which a vortex ring breaks down, as

$$t_c = \frac{3\Gamma}{16\pi\nu}\left(\frac{\rho a^3}{T}\right)^{1/2}. \tag{2.3}$$

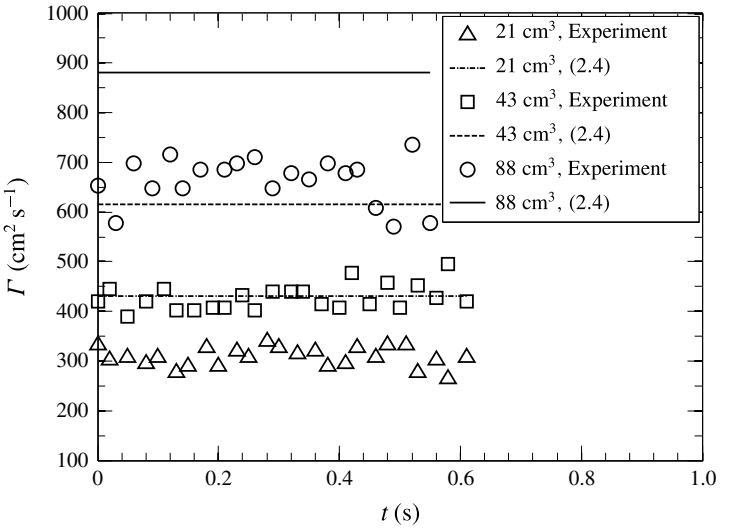

FIGURE 2. Circulation associated with three vortex ring bubbles with initial volumes of 21, 43 and 88 cm^3; symbols represent experimental results and lines correspond to the analytical prediction given by (2.4) (Walters & Davidson 1963). Maximum deviation corresponds to the case of 88 cm^3 for which relative standard deviation is approximately 7 %, indicating that circulation can be considered almost constant.

Equation (2.3) is valid only if the Weber number $We = \rho\Gamma^2/4\pi^2 aT$ is much larger than unity. In this equation, T stands for the surface tension of water in contact with air, and, ρ and ν are density and viscosity of water respectively. It must be considered that (2.3) is an implicit function since a is the core radius at the critical time and must be written in terms of t_c by combining ring volume $\Omega = 2\pi R(\pi a^2)$ with (2.1). For the vortex ring bubbles produced by bursting balloons we found a trend similar to that predicted by (2.3), i.e. as the circulation increases the bubble becomes more stable (see § 5).

Similar to Turner's (1957) theory, constant circulation is an essential assumption for Pedley's (1968) analysis. By deriving a similarity scale, Pedley demonstrated that the time required for vorticity to diffuse to the ring symmetry axis or to the boundary of the rotational flow region $\boldsymbol{B}$ (see figure 1) is on the order of a^2/ν, which is much greater than the critical time t_c. Hence, before the vorticity starts being cancelled across the symmetry axis or being swept off into a wake, the vortex ring becomes unstable and breaks down; upholding the assumption of vorticity conservation and, consequently, constant circulation. The assumption of constant circulation was also experimentally verified by Walters & Davidson (1963). They generated three vortex ring bubbles with volumes of 21, 43 and 88 cm^3 by rapidly releasing a jet of air at the bottom of a water tank. The circulations associated with these bubbles are reproduced in figure 2; relative standard deviation of each case is approximately 7 % indicating that the circulation can be considered roughly constant. In addition to experiments, Walters & Davidson (1963) applied the initial-motion theory to analytically investigate the motion of a vortex ring bubble, assuming it is initially spherical and starts from rest. They found a rough approximation of the circulation in terms of the initial volume Ω_0 as

$$\Gamma = 3g^{1/2}\Omega_0^{1/2}. \tag{2.4}$$

As illustrated in figure 2, the circulation obtained from (2.4) is roughly in accordance with their experimental measurements; we also found satisfactory agreement between circulations of bubbles produced by the bursting balloons and values determined from (2.4) (see § 5.1). In addition to the circulation, Walters & Davidson (1963) investigated the rising velocity. According to them, the bubble starts rising with twice the acceleration of gravity; however, as it travels upward it slows down.

Although numerical simulation of the generation and the translation of an air-core vortex ring is technically challenging, a few in-depth CFD analyses such as those of Lundgren & Mansour (1991) and Cheng *et al.* (2013) have been performed, revealing interesting details of the phenomenon. Lundgren & Mansour (1991) conducted a two-stage numerical simulation using a boundary integral method. In the first stage, it was observed that a liquid jet penetrated through the bubble from below until it impinged on the upper surface and generated a toroidal geometry. Owing to the complicated physics involved in the impingement, they could only continue the simulation until the liquid jet penetrated very close to the upper surface. Then, the second stage of the simulation started from a toroidal bubble, the initial circulation of which was determined from the first stage. Lundgren & Mansour (1991) improved Turner's (1957) results by solving the force balance equation,

$$\rho A \frac{\mathrm{d}\boldsymbol{u}}{\mathrm{d}t} = \rho \Gamma \, \widehat{\boldsymbol{e}}_t \times \boldsymbol{u} + \rho A g \, \widehat{\boldsymbol{e}}_z + \boldsymbol{F}_T \tag{2.5}$$

where $\boldsymbol{u}$ is velocity of an arbitrary point on the perimeter of the ring relative to the rising velocity of the ring, A is the cross-section area, $\widehat{\boldsymbol{e}}_t$ is the unit vector in the tangential direction and $\widehat{\boldsymbol{e}}_z$ is the unit vector in the vertical direction. The left-hand side of (2.5) represents the inertia and the right-hand side terms are Kutta–Joukowski lift, buoyancy and surface tension forces respectively. Having no viscous force in the force balance equation is supported by the aforementioned assumptions made by Turner (1957); also see the note by Sirakov, Greitzer & Tan (2005) on irrotational viscous flow. Solving (2.5) yields

$$R = R_T - \frac{1}{\Gamma^2}\frac{4}{9}\frac{\sin\tau}{R_T^{1/2}R_0^{3/2}} \tag{2.6}$$

where $\tau = (3/4)\Gamma^2(R_T^3 - R_0^3)$. Equation (2.6) corrects Turner's (1957) radius (2.1) by introducing a sinusoidal term; note the inverse effect of the initial condition (R_0) on the amplitude of oscillations. Although this equation suggests no phase difference in oscillations of the fluid particles located on the ring perimeter, it seems to be related to the azimuthal waves described by Krutzsch (1939) and Maxworthy (1972); this was confirmed by Lundgren in a private communication. We believe the energy consuming oscillations described by (2.6) may be a reason for the continuous decrease in the rising velocity of a vortex ring bubble.

3. Model

In this section, the model developed by Sullivan *et al.* (2008) is first recapitulated and then reformulated to be applicable to buoyant vortex rings. At the outset, consider the following equations, respectively for impulse P, energy E and velocity V of vortex rings:

$$P = \rho \Gamma \pi R^2, \tag{3.1}$$

$$E = \frac{1}{2}\rho\Gamma^2 R\left(\ln\left(\frac{8R}{a}\right) - \alpha\right), \tag{3.2}$$

$$V = \frac{\Gamma}{4\pi R}\left(\ln\left(\frac{8R}{a}\right) - \beta\right). \tag{3.3}$$

Parameters α and β depend on the core models; for viscous cores they are 2.040 and 0.558 while for solid rotating cores they are 7/4 and 1/4 respectively.

3.1. *Sullivan et al.'s (2008) model*

Based on their experiments, Sullivan *et al.* (2008) constructed a mathematical model for vortex rings generated by fast ejection of fluid via a piston/cylinder mechanism, namely a vortex gun. Accordingly, the momentum of the fluid displaced by the piston P_P was assumed to be equal to the impulse of the vortex ring P_V. Using (3.1)

$$\rho\Gamma\pi R^2 = \rho\pi R_0^2 L V_P \tag{3.4}$$

where R_0, L, V_P and R are the initial radius of the piston, length of the cylinder, velocity of the piston and radius of the vortex ring respectively. Thus, the circulation can be expressed in terms of vortex gun parameters as

$$\Gamma = \frac{R_0^2 L V_P}{R^2} \tag{3.5}$$

suggesting that the circulation increases with the volume of the cylinder and the velocity of the piston.

In addition to the circulation, Sullivan *et al.* (2008) modelled the slowing down of the vortex ring by considering the concept of drag. Drag force causes the impulse of the vortex ring to decrease as given by

$$\frac{\mathrm{d}P}{\mathrm{d}t} = -D_f = -C_d\frac{1}{2}\rho V^2 4\pi a R \tag{3.6}$$

where C_d is the drag coefficient, V is the rise velocity, a is the radius of the core and R is the radius of the vortex ring. Combining (3.1), (3.3) and (3.6) yields the following homogeneous differential equation:

$$\frac{\mathrm{d}V}{\mathrm{d}t} = \frac{\Lambda a}{2\pi R^2} C_d V^2 \tag{3.7}$$

in which $\Lambda = \ln(8R/a) - \beta$. Solving (3.7) for the rise velocity yields

$$V = \frac{V_0}{1 + V_0 c t} \tag{3.8}$$

where V_0 is the initial velocity of the vortex ring and c is the decay coefficient defined as $c = \Lambda a C_d/2\pi R^2$. One fundamental assumption to obtain (3.8) is that the radius of the vortex ring does not vary as it travels through the fluid. It is worth noting that for long times (3.8) agrees with the Maxworthy's (1972) prediction that the rising velocity decreases as t^{-1}.

3.2. *Modified model*

Unlike the approach adopted by Sullivan *et al.* (2008), it is not possible to construct a model for a vortex ring bubble produced by an underwater bursting balloon through the impulse (3.1), since there is no moving piston to equate its momentum to the initial impulse of the vortex ring. Instead, one can assume that the initial energy of the vortex ring bubble is equal to the potential energy of compressed air stored in the underwater balloon. Assuming an isothermal compression process, the potential energy stored in the balloon is given by

$$U_c = P_0 \Omega_0 \ln\left(\frac{P_{amb}}{P_0}\right) \tag{3.9}$$

where P_0, Ω_0 and P_{amb} are initial pressure of the balloon, initial volume of the balloon and ambient pressure respectively. Equating this to (3.2) gives

$$\tfrac{1}{2}\rho \Gamma^2 R(\ln(8R/a) - \alpha) = P_0 \Omega_0 \ln\left(\frac{P_{amb}}{P_0}\right). \tag{3.10}$$

Considering $P = \rho g h$ and $\Omega = 4\pi r^3/3$, (3.10) can be written as

$$\Gamma = \left(\frac{8\pi g}{3} \frac{r_0{}^3 (h_0 + h_{amb}) \ln\left(\dfrac{h_{amb}}{h_0}\right)}{R_0 \Lambda'}\right)^{1/2} \tag{3.11}$$

where $\Lambda' = \ln(8R_0/a) - \alpha$, h_0 is the initial depth of the underwater balloon, h_{amb} is the atmospheric pressure in meters of water, R_0 is the initial radius of the vortex ring and r_0 is equal to the radius of a perfect sphere enclosing the same volume of air, namely equivalent radius. An interesting analogy can be drawn between (3.5) and (3.11). Equation (3.5) suggests that the circulation of the vortex ring produced via a piston/cylinder mechanism depends on the displacement volume of the cylinder and the velocity of the piston, whereas according to (3.11), the circulation of the vortex ring produced by an underwater bursting balloon depends on the volume of the balloon and the depth at which the balloon bursts. Therefore, the effect of balloon volume is similar to the effect of cylinder volume and the effect of bursting depth is similar to the effect of piston velocity; both cause the circulation to increase. Moreover, (3.11) agrees well with (2.4), demonstrating that the circulation of the vortex ring is a function of $\Omega_0^{1/2}$.

To model the slowing down of the vortex ring we add the buoyancy force F_B to Sullivan *et al.*'s (2008) force balance equation (3.6) to give the following inhomogeneous differential equation:

$$\frac{\mathrm{d}P}{\mathrm{d}t} = -D_f + F_B = -C_f \frac{1}{2}\rho V^2 4\pi a R + F_B \tag{3.12}$$

in which C_f is the force coefficient representing all effective forces including viscous force, Kutta–Joukowski lift force, surface tension force etc., except buoyancy force. We can start solving (3.12) from the assumption made by Sullivan *et al.* (2008) that the radius of the vortex ring does not significantly change with time. Accordingly, the rise velocity converges to the constant value of $V = \sqrt{\pi a g / C_f}$ for long times. Although this solution qualitatively confirms the solution offered by Joseph *et al.*

(2007), it is in contrast with our preliminary experimental observations. The disparity is due to the assumption of constant radius. To resolve this, the radius is considered to be a time-dependent variable. The circulation, however, is assumed to be constant on the basis of (2.4) and (3.11). The validity of this assumption is further confirmed by our experimental measurements presented in § 5.1. Combining (3.12) with (3.1) and (3.3) under the assumption of constant circulation yields

$$\frac{\mathrm{d}R}{\mathrm{d}t} = C_1 \frac{(\ln(C_2 R\sqrt{R}) - \frac{1}{4})^2}{R^2\sqrt{R}} + \frac{C_3}{R} \tag{3.13}$$

where $C_1 = -\sqrt{6}\Gamma C_f/48\sqrt{\pi^5}$, $C_2 = 4\sqrt{6\pi}$ and $C_3 = F_B/2\pi\Gamma$. All parameters appearing in (3.13), including those with dimension of length, time, velocity, circulation and force, are normalized using r_0, $(r_0/g)^{1/2}$, $(gr_0)^{1/2}$, $(gr_0^3)^{1/2}$ and $\rho g r_0^3$ respectively, where ρ is the density of water, g is the gravitational acceleration and r_0 is the equivalent radius.

Although (3.13) is highly nonlinear with no general solution, one can produce a semi-analytical solution for any specific case by expanding the Taylor series for the right-hand side of the equation. Substituting the calculated radius into (3.3) yields the rise velocity. As a preliminary analysis, basic scaling can be used to qualify the solution of (3.13) by estimating the order of magnitude of each term. Note that the value of the dimensionless radius R in (3.13) is always larger than unity, i.e. the radius of the vortex ring bubble is always larger than the equivalent radius of the balloon r_0. Therefore, on the right-hand side, the order of magnitude of the second term, i.e. buoyancy term, is significantly greater than the order of magnitude of the first term, i.e. viscous term, since the exponent of radius in the denominator of the second term is smaller than that of the first term. It is worth mentioning that the disparity between the order of magnitude of the viscous term and that of the buoyancy term on the right-hand side of (3.13) increases with time, since these terms are inversely correlated to the ring radius and the vortex ring bubble expands as it rises.

It is now noteworthy to recall (2.5). Lundgren & Mansour (1991) did not include a drag force in this equation on the basis of Pedley's (1968) theory that the vortex ring bubble is predicted to become unstable before the vorticity generated at the bubble surface diffuses through the boundary of the rotational region (see figure 1). Comparing the order of magnitude of the right-hand-side terms of (3.13) reveals that even if the vorticity diffuses into the surrounding fluid, the effect of the drag force is minimal in comparison with the buoyancy force. Equating the order of magnitude of the left-hand side of (3.13) with the order of magnitude of the dominant term of the right-hand side yields

$$\frac{\Delta R}{t} \sim \frac{C_3}{R}; \tag{3.14}$$

therefore,

$$\Delta R \sim \frac{F_B t}{2\pi\Gamma R}. \tag{3.15}$$

One immediate outcome of (3.15) is the direct relation between expansion of the vortex ring and buoyancy force. Accordingly, buoyancy force is what causes the radius of the vortex ring to increase; this clearly reveals why the radius of the non-buoyant vortex rings studied by Sullivan *et al.* (2008) did not increase with time. One important point to consider is that although no buoyancy force acts on the non-buoyant vortex rings, they still radially expand as they advance. According

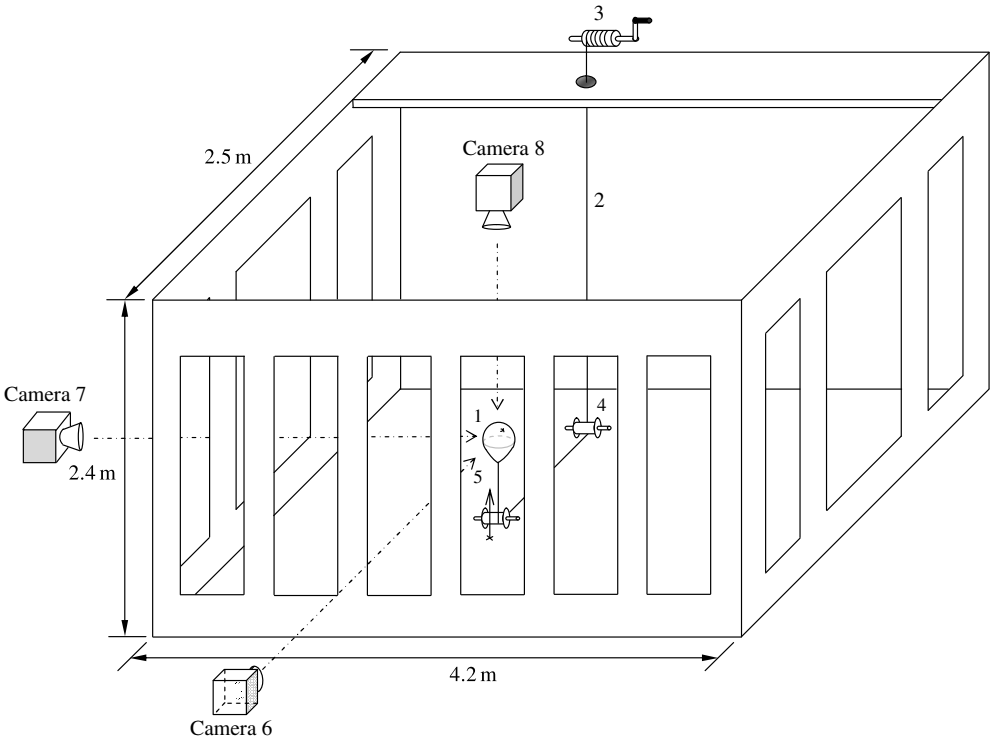

FIGURE 3. Sketch of the experimental setup: 1, balloon; 2, nylon line; 3, winch; 4, pulley system; 5, sharp needle; 6–8, cameras.

to (3.13), this expansion occurs under the action of viscous force and inertia, and is considerably lower than the radial expansion of a similar buoyant vortex ring. Solving (3.15) for radius R yields

$$R \sim R_0 + \left(R_0 + \frac{F_B t}{\pi \Gamma}\right)^{1/2}. \tag{3.16}$$

This order of magnitude is in good agreement with Turner's (1957) radius equation ((2.1); $R = (R_0^2 + Ft/\pi\Gamma)^{1/2}$). More is said regarding (3.11), (3.13), (3.15) and (3.16) in the results and discussion section (§ 5).

4. The experiment

The experiments reported in this study were conducted in a Plexiglas tank that was 4.2 m long, 2.5 m wide and 2.4 m high. The experimental setup is sketched in figure 3. As illustrated in this figure, an air-filled balloon (labelled 1) was gently pulled down via a thin nylon line (2) which was attached to a winch (3) through a pulley system (4). Once impressed on the sharp pin (5), the balloon burst and a vortex ring bubble was produced; a hypodermic needle with outer diameter of 0.4 mm was chosen as the pin. Similar to Hershberger *et al.* (2010), all the experimental data were obtained photographically. Three cameras (6–8) with speed of 60 f.p.s. at high resolution of 1080P were configured above and on two orthogonal sides of the tank to

record the generation and the motion of the vortex ring bubble. The videos were then analysed frame by frame using the MATLAB image processing toolbar to deduce the elevation and dimensions of the vortex ring bubble. The rate of expansion $\mathrm{d}R/\mathrm{d}t$ was calculated using the measured ring radius, and the rising velocity V was obtained from the measured elevation. Substituting the rising velocity and the dimensions of the ring in (3.3) yields the circulation as

$$\Gamma = 4\pi R\, V \left(\ln\left(\frac{8R}{a}\right) - \frac{1}{4}\right)^{-1}. \tag{4.1}$$

Similar to (3.13), all measured parameters including those with the dimension of length, time, velocity, acceleration and circulation were made dimensionless using r_0, $(r_0/g)^{1/2}$, $(gr_0)^{1/2}$, g and $(gr_0^3)^{1/2}$ respectively, where g is the gravitational acceleration and r_0 is the equivalent radius of the balloon.

The reciprocal of dimensionless surface tension, the so-called Bond number, given as

$$Bo = S^{-1} = \frac{\rho g r_0^2}{T}, \tag{4.2}$$

was chosen as the independent variable, where $T = 72.8 \times 10^{-5}$ N cm^{-1} is water–air surface tension at 20 °C. Results were reported for Bond numbers 225 ± 14, 500 ± 10, 750 ± 9 and 1000 ± 7, respectively associated with initial volumes of approximately 334, 946, 1740 and 2676 cm^3. Given uncertainties were obtained from the standard deviation of ten individual measurements at a 95 % confidence level. The initial volume of each balloon was measured through three independent approaches: Archimedes principle, the displacement volume of the balloon inflation pump through utilization of the Boyle–Mariotte law, and finally MATLAB image processing. The average of the three measurements was considered to represent the initial volume. Note that, alternatively, one could use dimensionless surface tension $S = T/(\rho g R_0^2)$ instead of Bond number; therefore, Bond numbers 225, 500, 750 and 1000 could be replaced with dimensionless surface tensions of 0.0040, 0.0020, 0.0013 and 0.0010, respectively.

5. Results and discussion

When a sufficiently large air-filled balloon quickly bursts underwater, a vortex ring bubble will be generated. Note that no vortex ring can be produced if the balloon is not large enough, since the associated small bubble will be easily suppressed by the punctured balloon. Likewise, if the air is released slowly, for instance if the balloon is ripped by a blunt pin, no vortex ring will be generated either, even if the balloon is large; this is similar to the case of tilting an inverted beaker as described by Lundgren & Mansour (1991). To ensure that the wall effects are negligible, the largest vortex ring bubbles included in this study were set to be approximately 2700 cm^3 with an associated dimensionless surface tension of $S = 0.0010$. This leads to a sufficiently low blockage ratio of approximately 1 %, assuming that the vortex ring and the bulk fluid region rising along with it is a bluff body. The smallest vortex ring bubbles we could produce in the tank described in figure 3 were approximately 335 cm^3 with an associated dimensionless surface tension of $S = 0.0040$. This is much larger than those generated with previous techniques; for instance, Walters & Davidson (1963) generated vortex rings with volume of 21 cm^3 by rapidly releasing a jet of air at the bottom of a water tank. In the conventional techniques the required upward

momentum to generate a vortex ring is provided by an external source, for instance a moving piston; therefore, even very small vortex rings can be generated if the input momentum has been sufficiently increased. However, the input momentum of a vortex ring generated by a bursting balloon is provided through the buoyancy force; when the initial volume of the balloon was less than approximately 335 cm^3 the buoyancy force appeared to be insufficient to provide the momentum required for the vortex ring generation.

For the case of $S = 0.0040$, the vortex ring appeared markedly unstable and broke down into small spherical cap bubbles after approximately 2.5 s at an elevation of approximately $z = 1.25$ m above the initial level of the balloon. According to Cheng *et al.* (2013) the number of spherical cap bubbles that a vortex ring bubble breaks into is equal to the number of azimuthal waves generated on the ring perimeter. In Cheng *et al.*'s (2013) simulation, the number of waves was set to be 8; in our experiments, however, it appeared to vary from run to run. Vortex ring bubbles with dimensionless surface tension of $S = 0.0020$, however, did not break down before reaching the free surface at $z = 2$ m. By decreasing the dimensionless surface tension to $S = 0.0013$ and then to $S = 0.0010$ vortex ring bubbles appeared to become progressively more stable and stronger, indicating that the lower dimensionless surface tension (i.e. higher Bond number) leads to a longer lasting vortex ring bubble. In other words, the lifetime of vortex rings appears to be limited by the amount of surface tension instability. This trend is consistent with (2.3) proposed by Pedley (1968), but in contrast with data reported by Cheng *et al.* (2013). According to Cheng *et al.* (2013), as the Bond number decreases, the vortex ring becomes more stable and its lifetime increases. It must be mentioned that their simulation was conducted over a very different range of $30 \leqslant Bo \leqslant 100$ which is notably smaller than the Bond number of the vortex ring bubbles studied herein. The vortex ring instability can also be attributed to the oscillations described by (2.6). The amplitude of those destructive oscillations is directly proportional to the dimensionless surface tension; therefore, when the dimensionless surface tension increases, the vortex ring will be subjected to stronger oscillations, consequently, it will not survive as long. The azimuthal waves described by Krutzsch (1939) and Maxworthy (1972) could be cited as another reason for vortex ring breakdown. In addition, the process of destabilization is presumably accelerated by external influences, for instance the punctured balloon, which is entrained by the vortex and subsequently marks ring rotations at the bubble surface as it travels with it. There is also slight distortion caused by the pin at the instant of bursting.

In the following sections the radius, the trajectory, the circulation, the rise velocity and the energy balance of the vortex ring bubbles generated by a bursting balloon are investigated over the range of $S = 0.0010$–0.0040.

5.1. *Circulation*

In contrast to the vortex ring guns where the circulation is produced by viscous separation at the exit hole (Maxworthy 1972), the circulation associated with a vortex ring produced by a bursting balloon is generated by the inertial process of the toroid formation through which a gravitationally driven liquid tongue penetrates upward into the droplet-shaped bubble from the bottom, impinges on the upper surface and escapes out of the bubble; this makes the fluid rotate around an imaginary axis forming the vortex ring bubble. Figure 4 attempts to illustrate the described process via a time-sequence of frames: (*a*) corresponds to the moment just after the bursting, and (*j*) shows the approximate moment at which the vortex ring is formed. Due to the opaque surface of the bubble it is difficult to visualize the penetrating tongue.

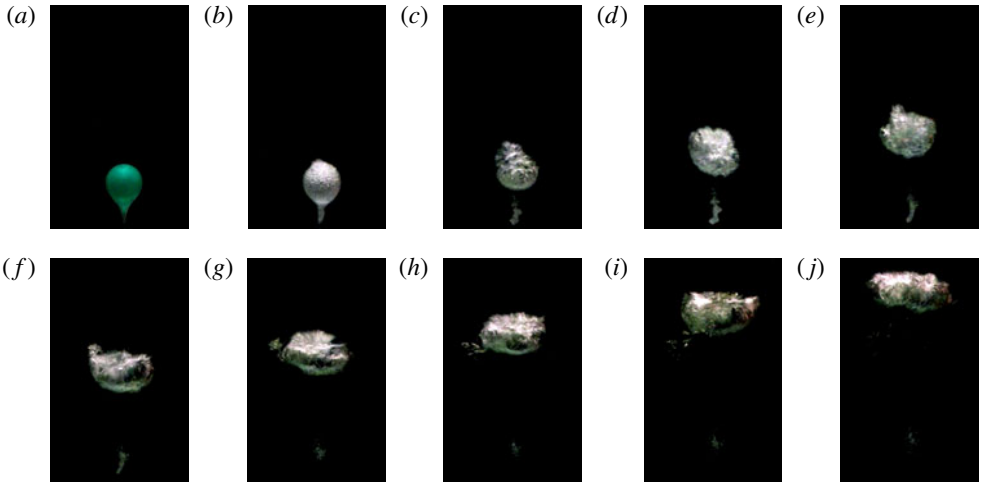

FIGURE 4. (Colour online) Vortex ring bubble formation, $S = 0.0010$: (*a*) $t = 0$ s, (*b*) $t = 1/30$ s, (*c*) $t = 3/30$ s, (*d*) $t = 5/30$ s, (*e*) $t = 7/30$ s, (*f*) $t = 9/30$ s, (*g*) $t = 11/30$ s, (*h*) $t = 13/30$ s, (*i*) $t = 15/30$ s, (*j*) $t = 17/30$ s.

Figure 5 compares circulations associated with different dimensionless surface tensions; these values are calculated using (4.1). It is observed that circulation increases as the Bond number, i.e. the balloon size, increases. This observation agrees well with what was predicted by (3.11), according to which at a specific depth the circulation of the vortex ring directly depends on the initial volume of the balloon. In other words, a greater initial potential energy causes circulation to increase. This is logically consistent with the case of a vortex ring gun where circulation increases with the speed of the piston, i.e. higher initial kinetic energy (Sullivan *et al.* 2008). In other words, regardless of the technique used to produce the vortex ring, circulation is a direct function of the initial amount of energy. As is seen, at a specific dimensionless surface tension, circulation is approximately constant with respect to time; maximum relative standard deviation is approximately 6 % which is lower than that associated with Walters & Davidson's (1963) measurements (see figure 2).

Measured circulations are compared with those estimated by (2.4); fairly good agreement is found. The disparity can be attributed to the basic assumption made in the derivation of this equation that the bubble is initially spherical, whereas in our experiments the bubble was initially droplet shaped. It is of note to mention that the experimental results here compare much better with (2.4) than those of Walters & Davidson (1963); this is likely to be due to the completely different test conditions and vortex generation techniques (see figure 2). As is observed in figure 5, measured circulations are also consistent with those from (3.11). The overestimation is due to the assumption underlying this equation: that the initial potential energy stored in the balloon entirely converts to the kinetic energy of the vortex ring. In other words, viscous dissipation from the moment of bursting (see figure 4*a*) to the moment of vortex ring formation (see figure 4*j*) is not taken into account. Hence, calculating the difference between the energy associated with the measured initial circulation and the energy associated with the circulation estimated through (3.11) yields the amount of energy dissipated during the vortex ring formation process. For dimensionless surface

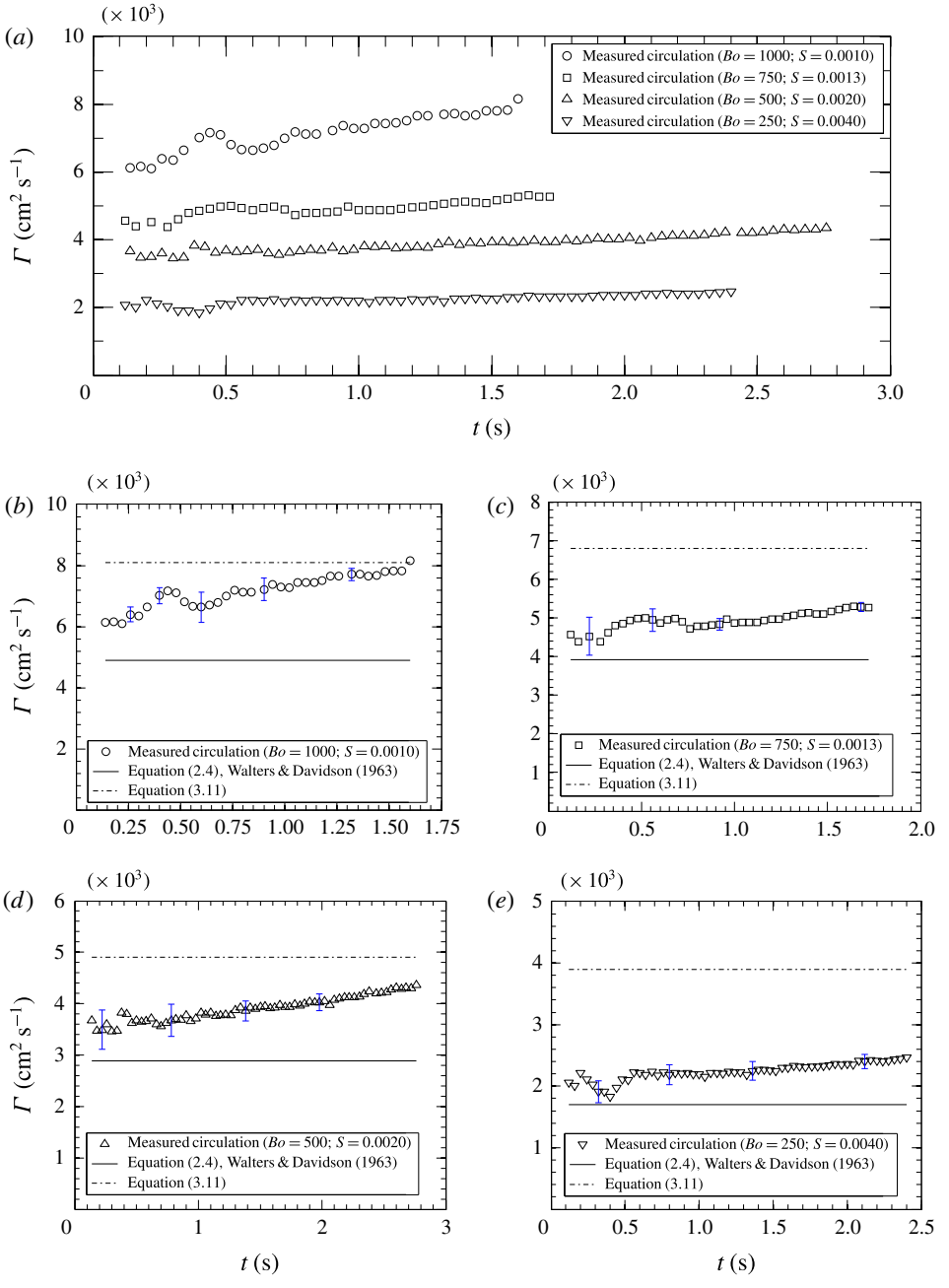

FIGURE 5. (Colour online) Circulation associated with dimensionless surface tensions ranging from $S = 0.0010$ to $S = 0.0040$; symbols represent measured values, lines show values estimated through (2.4) and predicted by (3.11).

tension of 0.0010, almost 50 % of the initial potential energy stored in the balloon was found to be dissipated during the vortex ring bubble formation; this value was increased to 70 % for dimensionless surface tension of 0.0040.

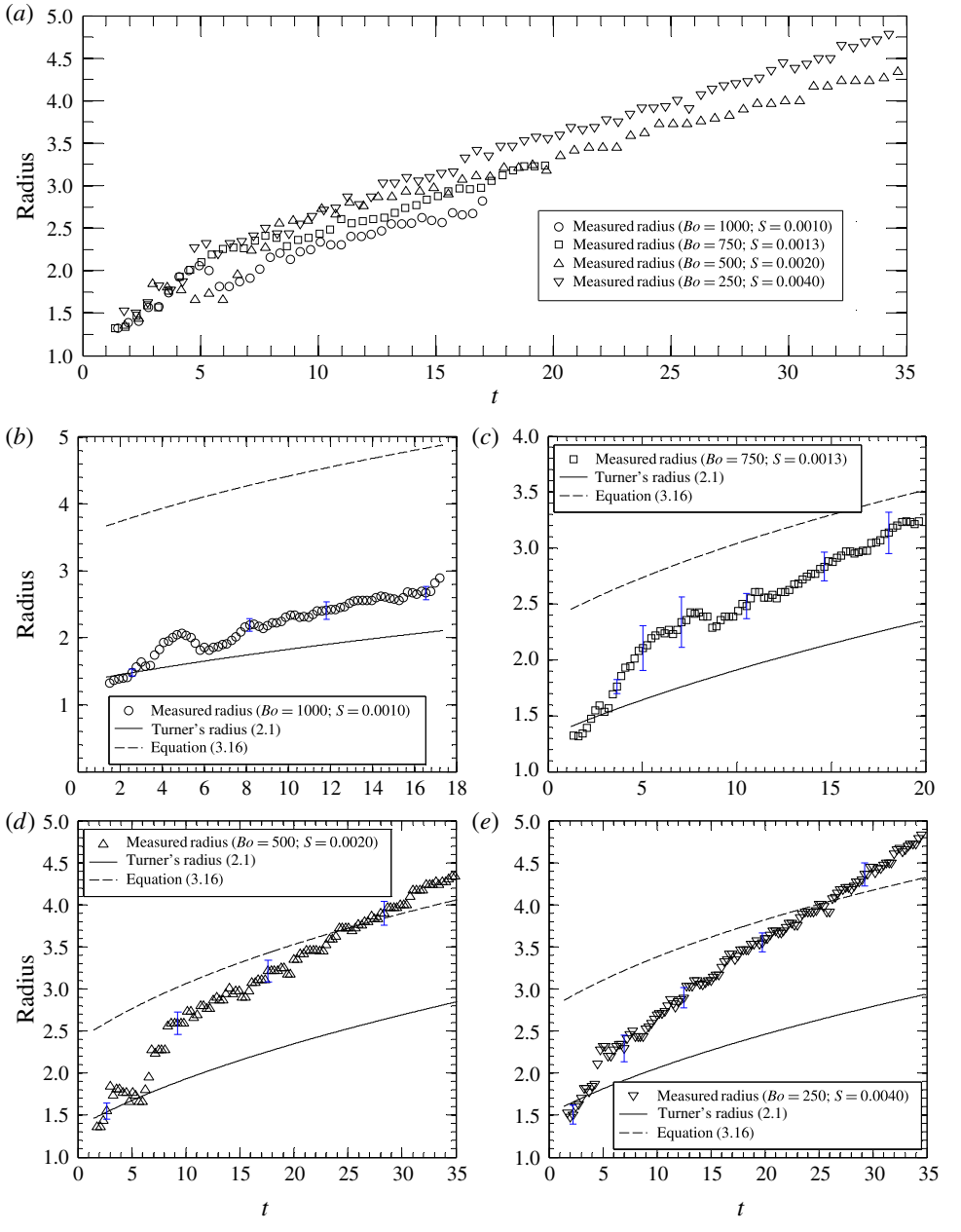

FIGURE 6. (Colour online) (*a*) Influence of dimensionless surface tension on the dimensionless vortex ring radius. (*b–e*) Comparing measured radius of vortex ring bubbles with values predicted by (2.1) and (3.16).

5.2. *Radius*

The effect of dimensionless surface tension on the radius of vortex ring bubbles is illustrated in figure 6. As is observed in figure 6(*a*), at a fixed dimensionless surface tension, the vortex ring radius increases with time. Figure 6(*b–e*) compares measured ring radius with the Turner's (1957) radius (2.1); a good qualitative agreement is

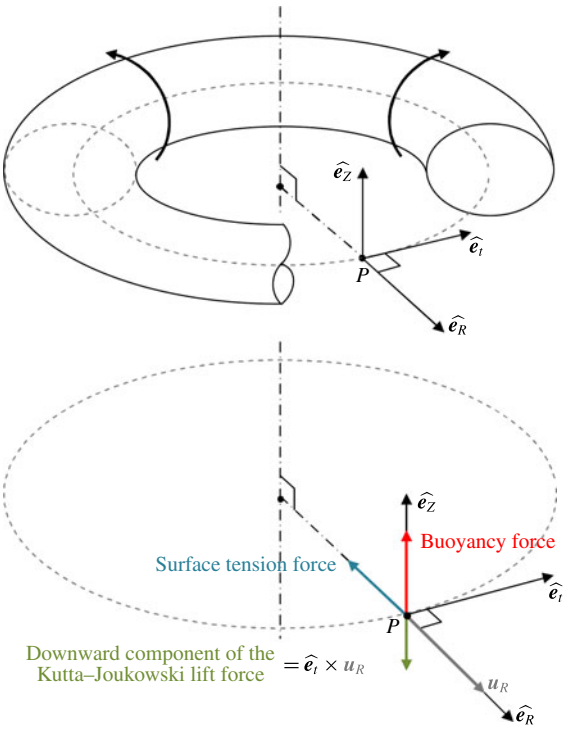

FIGURE 7. (Colour online) The radial expansion of the vortex ring bubble, $\boldsymbol{u}_R$, leads to a downward Kutta–Joukowski lift force, $\widehat{\boldsymbol{e}}_t \times \boldsymbol{u}_R$, which is necessary to balance the buoyancy force and inertia effect.

observed. Measured data were also compared with the order of magnitude given by (3.16); although this equation was obtained from a very simple basic-scaling analysis it appeared to predict the ring radius as well as Turner's (1957) equation. Although the experiment was carefully controlled to minimize the effect of the initial conditions, the repeatability needs to be assessed by estimating the precision of individual measurements. Error bars shown in figure 6(*b–e*) represent precision of ten individual measurements at a 95 % confidence level. For visual clarity, error bars are shown only on typical data points. As is suggested by (3.15) the radial expansion of the vortex ring bubbles is essentially due to the buoyancy force. According to (3.15), one expects to see a one order-of-magnitude change in the rate of expansion by increasing the dimensionless surface tension from 0.0010 to 0.0040 since the buoyancy force decreases approximately 10 times. It is observed that the dimensionless radius increases with the dimensionless surface tension; the rate of expansion, however, appeared to remain constant. This is due to the inverse correlation of circulation with the rate of expansion; as was observed in figure 5, circulation increases with the buoyancy force. In addition to (3.15), the underlying physics of the ring expansion can also be explained using (2.6) proposed by Lundgren & Mansour (1991). Considering the upward buoyancy force and the radially inward surface tension force, a downward component of the Kutta–Joukowski lift force must exist, since the bubble rises with a negative acceleration (see (2.2)). As is illustrated in figure 7, to have a downward Kutta–Joukowski lift force there must be a radial velocity component $\boldsymbol{u}_R$, demonstrating the radial expansion of vortex ring bubbles.

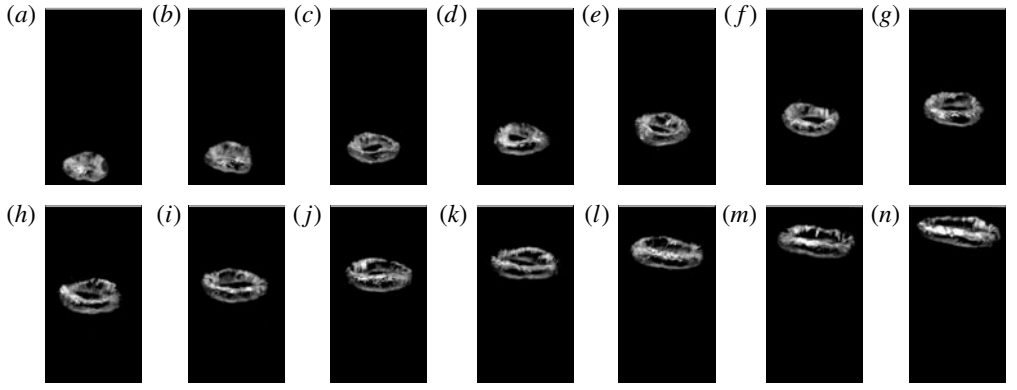

FIGURE 8. Translation of the vortex ring bubble corresponding to the case of $S = 0.0010$. This corresponds to later times of the vortex ring illustrated in figure 4: (*a*) $t = 17/30$ s, (*b*) $t = 19/30$ s, (*c*) $t = 21/30$ s, (*d*) $t = 23/30$ s, (*e*) $t = 25/30$ s, (*f*) $t = 27/30$ s, (*g*) $t = 29/30$ s, (*h*) $t = 31/30$ s, (*i*) $t = 33/30$ s, (*j*) $t = 35/30$ s, (*k*) $t = 37/30$ s, (*l*) $t = 39/30$ s, (*m*) $t = 41/30$ s, (*n*) $t = 43/30$ s.

It is worthwhile to mention that the small fluctuations of the ring radius observed in figure 6 can be attributed to the azimuthal waves described by Krutzsch (1939) and Maxworthy (1972). The mentioned fluctuations are more considerable at lower dimensionless surface tensions, particularly at early times. Figure 8 is an attempt to give a visual impression of these waves on the perimeter of a vortex ring bubble through a time-series of snapshots at $S = 0.0010$. Figure 8(*a*) represents the approximate moment at which the azimuthal waves were visualized for the first time, and figure 8(*n*) depicts the vortex ring at the moment that the free surface starts bowing; beyond this moment the vortex ring will be affected by the free surface (free surface is not shown in the figure). Note that the bubble depicted in figure 8 corresponds to early times of the vortex ring illustrated in figure 4.

5.3. *Trajectory*

Figure 9 illustrates the trajectory of the core centre of the vortex ring bubble at the dimensionless surface tensions studied herein. Note that the elevation and radius of each case have been made dimensionless using the corresponding equivalent radius r_0 (see § 4). As is observed, the trajectory of each case is roughly linear; the slope slightly decreases with the dimensionless surface tension. According to figure 9, as the dimensionless surface tension increases, the vortex ring bubble forms at a higher dimensionless elevation. Similarly, the larger dimensionless surface tension leads to a larger initial dimensionless radius.

5.4. *Rise velocity*

Figure 10 illustrates the effect of dimensionless surface tension on dimensionless rising velocity. As is observed, the rise velocity increases as the dimensionless surface tension decreases. It is also observed that at a fixed dimensionless surface tension, the rise velocity decreases with time. This trend is in agreement with Hick's equation (3.1). According to Hick's equation, and considering the fact that vortex rings expand as they rise, the rising velocity decreases with time. The velocity

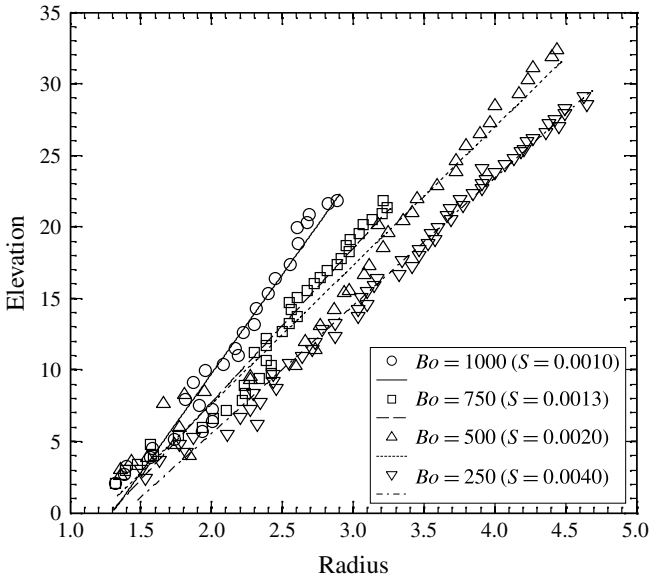

FIGURE 9. Effect of dimensionless surface tension on the trajectory of the core centre.

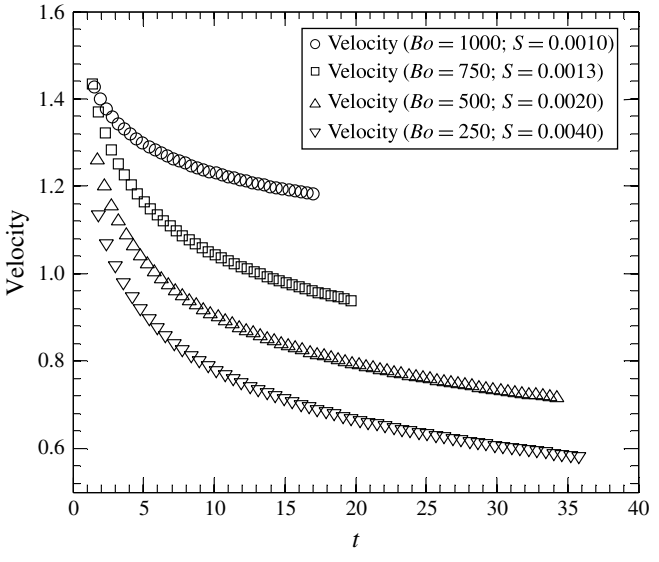

FIGURE 10. Effect of dimensionless surface tension on dimensionless rising velocity.

reduction illustrated in figure 10 also agrees with Turner's (1957) velocity u_T (2.2). A similar trend is observed in Walters & Davidson's (1963) experiments and Cheng *et al.*'s (2013) simulations.

A number of physical factors can be listed to explain the slowing down of vortex ring bubbles. This can be attributed to energy consuming oscillations described by (2.6); the energy of the oscillations is supplied from mechanical energy of the vortex ring; therefore, the total mechanical energy of the vortex ring decreases with time, causing deceleration. A similar interpretation can be made for those azimuthal waves

visualized in figure 8; waves extract energy from the vortex ring bubble, slowing its motion. Another suggestion is the entrainment process (Maxworthy 1972). Velocity depends upon the amount and distribution of vorticity, and due to the entrainment process, the vorticity generated at the bubble surface is distributed over a larger region of the bulk fluid as the bubble rises. This may cause a continuous reduction in the rise velocity. Viscous dissipation also is likely to be influential on the deceleration of the vortex ring bubbles.

To ensure the negligibility of the free surface tension, the rising velocity was measured over a fair distance away from the free surface. The rising velocity was calculated up to the level at which the free surface started bowing; beyond this point the vortex ring bubble will be affected by the free surface. It is worth noting that the rising velocity starts to decrease immediately after the vortex ring bubble is generated, where it is far below the free surface, so the slowing of the vortex ring bubble cannot be attributed to the effect of the free surface.

6. Conclusion

We have examined some of the basic dynamic features and stability characteristics of vortex ring bubbles. The primary motivations for this work were investigating flow generated by a balloon bursting underwater, modifying Sullivan *et al.*'s (2008) drag-based model to include buoyant vortex rings, and studying large vortex rings with Bond numbers up to 1000. Notable observations from the studied conditions are summarized as follows:

(*a*) A basic scaling analysis demonstrated that the significant radial expansion of vortex ring bubbles is essentially due to the buoyancy force. The effect of buoyancy in the momentum balance was found to be much greater than the effect of the viscous force; the difference was found to increase with time.

(*b*) An expression for the circulation was obtained according to which the circulation increases with the volume of the balloon and the depth at which the balloon bursts. Comparing the measured circulations with those predicted by this expression demonstrates the considerable viscous dissipation through the vortex ring formation process.

(*c*) For dimensionless surface tension of 0.0010, almost 50 % of the initial potential energy stored in the balloon was found to be dissipated during the vortex ring bubble formation; this value was increased to 70 % for dimensionless surface tension of 0.0040.

(*d*) Vortex ring bubbles were found to have a finite lifetime. As the dimensionless surface tension decreased, the structure of a vortex ring bubble became more coherent and it survived longer.

(*e*) It was observed that vortex ring bubbles expand as they rise. The rate of expansion appeared to remain approximately constant with respect to dimensionless surface tension.

(*f*) Non-dimensional radius was found to be larger as dimensionless surface tension increased.

(*g*) Circulation appeared to be inversely proportional to dimensionless surface tension. However, for a given dimensionless surface tension, it was approximately constant with respect to time. Vortex ring bubbles were found to decelerate as they rise. The rising velocity was faster at lower dimensionless surface tensions.

(*h*) The trajectory of the core centre of a vortex ring bubble was found to be approximately linear, with line slope slightly decreasing with dimensionless surface tension.

Acknowledgements

The authors are deeply indebted to Professors T. J. Pedley, T. Lundgren and R. Donnelly for their helpful comments. This work is made possible by the Natural Sciences and Engineering Research Council of Canada and the Ontario Trillium Foundation.

REFERENCES

CHENG, M., LOU, J. & LIM, T. T. 2013 Motion of a bubble ring in a viscous fluid. *Phys. Fluids* **25**, 1–19.

GAN, L., DAWSON, J. R. & NICKELS, T. B. 2012 On the drag of turbulent vortex rings. *J. Fluid Mech.* **709**, 85–105.

HERSHBERGER, R. E., BOLSTER, D. & DONNELLY, R. J. 2010 Slowing of vortex rings by development of Kelvin waves. *Phys. Rev.* E **82**, 036309.

JOSEPH, D., FUNADA, T. & WANG, J. 2007 *Potential Flows of Viscous and Viscoelastic Liquids*. Cambridge University Press.

KRUTZSCH, C. H. 1939 Ber eine experimentell Beobachtete Erscheinung an Wirbelringen bei ihrer translatorischen Bewegung in Wirklichen Flussigkeiten. *Ann. Phys. Berlin* **427** (6), 497–523.

LUNDGREN, T. S. & MANSOUR, N. N. 1991 Vortex ring bubbles. *J. Fluid Mech.* **224**, 177–196.

MAXWORTHY, T. 1972 The structure and stability of vortex rings. *J. Fluid Mech.* **51**, 15–32.

PEDLEY, T. J. 1968 The toroidal bubble. *J. Fluid Mech.* **32**, 97–112.

REYNOLDS, O. 1876 On the resistance encountered by vortex rings and the relation between the vortex rings and the streamlines of a disk. *Nature* **14**, 477–479.

SIRAKOV, B. T., GREITZER, E. M. & TAN, C. S. 2005 A note on irrotational viscous flow. *Phys. Fluids* **17** (10), 1–3.

SULLIVAN, I. S., NIEMELA, J. J., HERSHBERGER, R. E., BOLSTER, D. & DONNELLY, R. J. 2008 Dynamics of thin vortex rings. *J. Fluid Mech.* **609**, 319–347.

TURNER, J. S. 1957 Buoyant vortex rings. *Proc. R. Soc. Lond.* A **239**, 61–75.

WALKER, J. D. A., SMITH, C. R., CERRA, A. W. & DOLIGALSKI, T. L. 1987 The impact of a vortex ring on a wall. *J. Fluid Mech.* **181**, 99–140.

WALTERS, J. K. & DAVIDSON, J. F. 1963 The initial motion of a gas bubble formed in an inviscid liquid. *J. Fluid Mech.* **17**, 321–336.